SWORD M-SCH-B2735 - P-RICH IRON - IRON AGE - SWITZERLAND

Artefact name	Sword M-Sch-B2735
Authors	Marianne. Senn (EMPA, Dübendorf, Zurich, Switzerland) & Christian. Degrigny (HE-Arc CR, Neuchâtel, Neuchâtel, Switzerland)
Url	/artefacts/222/

The object

Credit HE-Arc CR.

Fig. 1: Iron sword (after Senn Bischofberger 2005, 241),

Description and visual observation

Description of the artefact	Sword of the middle la Tène type, broken into two parts (Fig. 1). Under a hand lens the surface shows parallel grinding traces from mechanical cleaning.
Type of artefact	Weapon
Origin	Marin-Epagnier, La Tène, Saint-Blaise, Neuchâtel, Switzerland
Recovering date	Water finds, end 19th/beginning 20th cent. AD
Chronology category	Iron Age
chronology tpq	250 B.C.
chronology taq	140 B.C.
Chronology comment	La Tène C, 250 _ 140 BC
Burial conditions / environment	Soil
Artefact location	Museum Schwab, Biel/Bienne, Bern
Owner	Museum Schwab, Biel/Bienne, Bern
Inv. number	M-Sch-B2735
Recorded conservation data	Conserved (not recorded, but mechanical cleaning visible)

Study area(s)

Credit HE-Arc CR.

Fig. 2: Location of sampling area,

Binocular observation and representation of the corrosion structure

Stratigraphic representation: none

MiCorr stratigraphy(ies) – Bi

Sample(s)

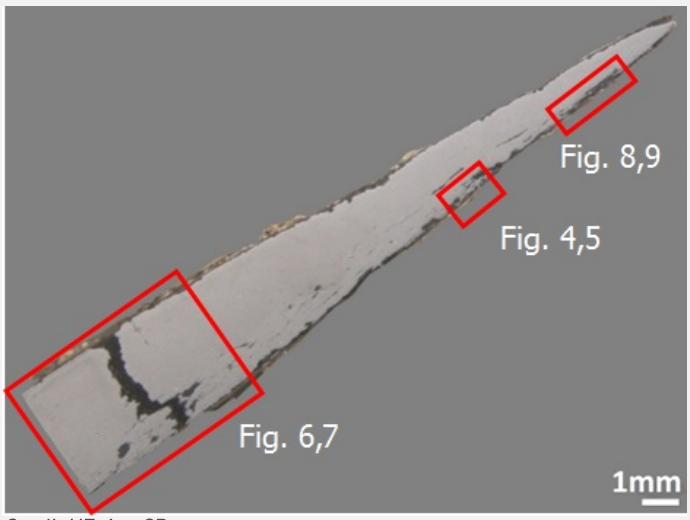

Credit HE-Arc CR.

Fig. 3: Micrograph of the cross-section showing the locations of Figures 4 to 9,

Description of sample	The sample includes half of the sword blade. The corrosion layer is thin.
Alloy	P-rich iron
Technology	Forged, annealed and cold worked
Lab number of sample	M-SCH-B2735
Sample location	Empa (Marianne Senn)
Responsible institution	Schweizerisches Landesmuseum, Zürich, Zurich
Date and aim of sampling	1969, metallography

Analyses and results

Analyses performed:
Metallography (nital etched), Vickers hardness testing, LA-ICP-MS, SEM/EDX.

Non invasive analysis

Metal

The remaining metal is a P-rich (0.2 mass%) iron (Table 1) with long parallel slag inclusions (Fig. 4) concentrated on one side of the blade. The slag inclusions are composed of wüstite/FeO dendrites and fayalite/Fe_2SiO_4 in a glassy matrix (Fig. 5 and Table 2). Their chemical composition is typical for iron produced by the bloomery process (dominated by iron oxides and silica). It is difficult to identify the ore type from the slag composition. Interestingly in one case the slag composition is very specific (alumina and P-rich material). After etching, the metal shows a ferritic structure (Fig. 6). The grain size is variable (between ASTM grain sizes of 4 to 7) and some grains include Neumann bands (Fig. 7). A large crack has developed through the metal section (Figs. 3 and 6). The average hardness of the metal (HV1 185) is quite high for a wrought iron. The level of hardness and Neumann bands are typical for a P-rich iron. Neumann bands are said to develop by cold working and shock deformation. According to Swiss and McDonnell 2003 they form when little cold work is carried out. Distortion (grain deformation) after cold working starts to be apparent in iron after a reduction in thickness of between 30-40%. Since no grain deformation is visible, the present reduction is probably a little less than this range.

Elements	V	Cr	Mn	P	Co	Ni	Cu	As	Ag
Median mg/kg	<	5	10	2200	140	270	500	260	<
Detection limit mg/kg	1	4	1	50	1	1	1	2	0.1
RSD %	-	56	48	10	14	16	37	15	-

Table 1: Chemical composition of the metal. Method of analysis: LA-ICP-MS, Lab Analytical Chemistry, Empa (for details see Devos et al. 2000).

Location	MgO	Al_2O_3	SiO_2	P_2O_5	K_2O	CaO	TiO_2	MnO	FeO	Total	SiO_2/Al_2O_3
Wüstite in glass	0.7	2.1	15	2.7	<	0.6	<	<	87	109	7.2
Wüstite and fayalite in glass	<	4.8	24	0.7	1	1.4	<	<	70	103	5.0
Wüstite and fayalite in glass	0.6	2.7	23	1.8	<	0.8	<	<	69	98	8.4
Fayalite in glass	<	5.6	26	2.8	0.8	1.4	<	<	72	110	4.8
Fayalite phase	0.8	1.0	31	1.2	0.7	1.1	<	0.8	69	106	33
Fayalite in glass	<	8.8	24	3.2	1.0	1.4	0.6	<	66	106	2.8

Table 2: Chemical composition of the slag inclusions (mass%) at the tip (pearlite) and the body (ferrite) of the knife. Method of analysis: SEM/EDX, Laboratory of Analytical Chemistry, Empa.

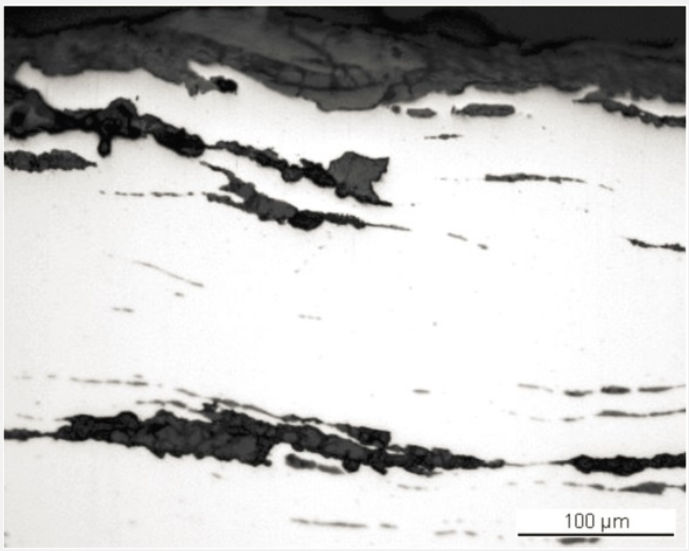

Credit HE-Arc CR.

Fig. 4: Micrograph of the metal sample from Fig. 3 (detail, rotated by 225°), unetched, bright field. In white the metal containing elongated slag inclusions (in grey); in black porosity,

Fig. 5: Micrograph of the metal sample from Fig. 3 (detail), unetched, bright field. Detail with slag inclusions showing a structure with wüstite dendrite (light-grey) and fayalite (dark-grey),

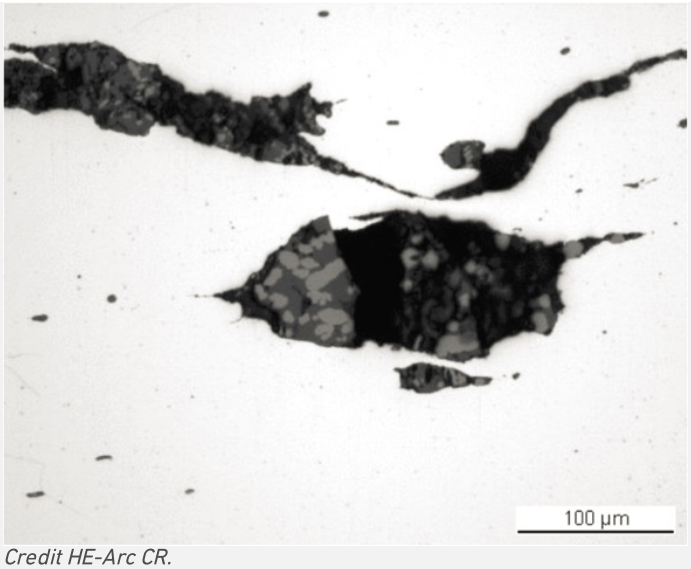

Credit HE-Arc CR.

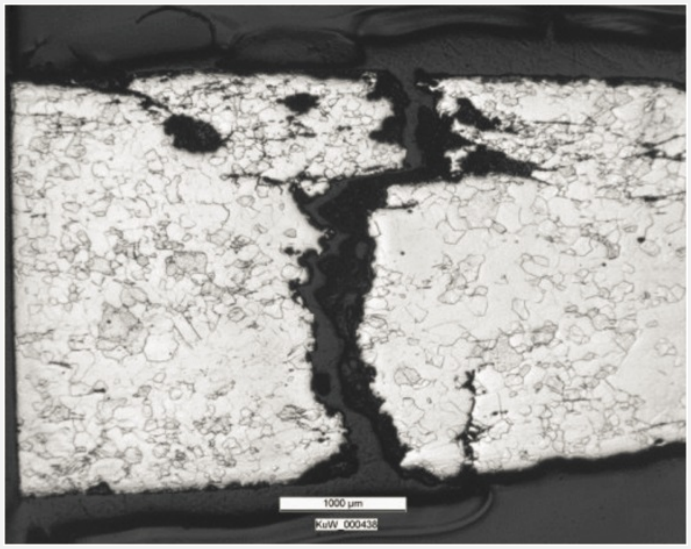

Credit HE-Arc CR.

Fig. 6: Micrograph of the metal sample from Fig. 3 (reversed picture, rotated by 225°, detail), etched, bright field. Metal with a large pre-existing crack and ferritic, recrystallized structure. Grains have different sizes,

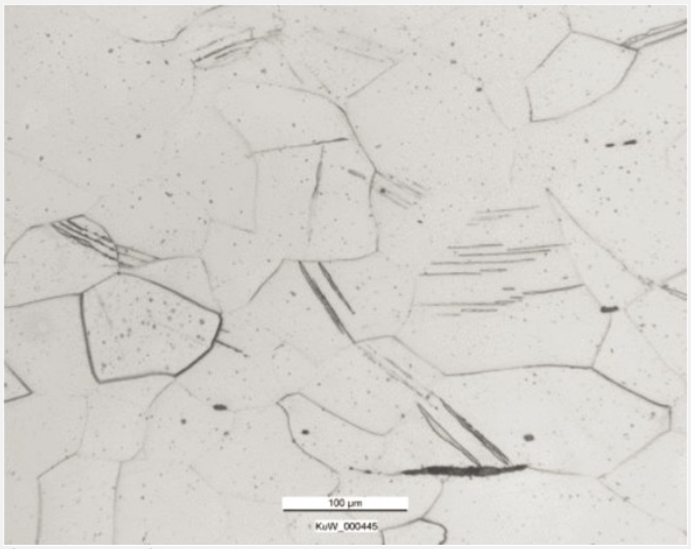

Credit HE-Arc CR.

Fig. 7: Micrograph (detail of Fig. 6), etched, bright field. Ferrite grains including Neumann bands formed after cold working in a P-rich iron,

Microstructure	Recrystallized grains, Newman bands, ghost structure
First metal element	Fe
Other metal elements	

Corrosion layers

The remaining metal, including the large crack, is covered by a thin, fissured corrosion crust (Figs. 3, 4, 5 and 9). The corrosion crust is thicker on the side containing the long slag inclusions (Fig. 3). In bright field and in the BSD-mode of the SEM image only light and dark-grey areas can be distinguished (Figs. 4 and 9). Under polarised light the corrosion products appear yellow-orange near the metal surface and then become successively dark-red and black. The outer layer is orange-yellow, as is the inner one (Fig. 8). There is a correlation between the level of grey in SEM/BSD-mode, the colours under polarised light, and the chemical composition of the corrosion layer (Table 3, Figs. 8 and 9). The lighter the grey of the SEM/BSD-mode, or the colours (light-brown and red) under polarised light, the richer the area is in Fe and the more depleted it is in O. Surprisingly the inner corrosion layer is contaminated with Si, Al and O.

Elements	O	Si	Fe	Total
Light or dark-red corrosion products (CP3i)	25	1.6	67	94
Light or dark-red corrosion products (CP3i)	32	<	74	108
Dark or dark-red corrosion products (CP2i)	41	<	67	109

Table 3: Chemical composition (mass %) of the corrosion layer (from Fig. 8). Method of analysis: SEM/EDX, Laboratory of Analytical Chemistry, Empa.

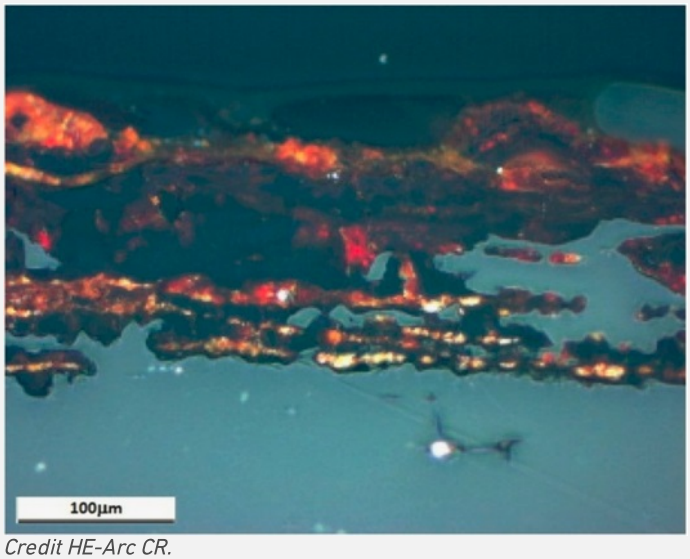

Credit HE-Arc CR.

Fig. 8: Micrograph showing the metal - corrosion crust interface from Fig. 3 (inverted picture, rotated by 135°, detail), unetched, polarised light. The metal appears in blue and the corrosion changes from yellow-orange to dark-red and black,

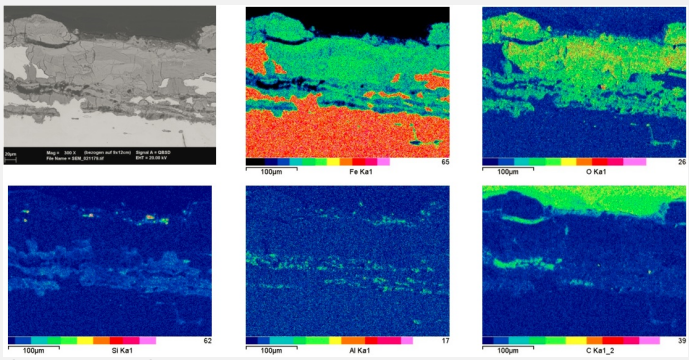

Credit HE-Arc CR.

Fig. 9: SEM image, BSD-mode, and elemental chemical distribution of the selected area from Fig. 8. Method of examination: SEM/EDX, Laboratory of Analytical Chemistry, Empa.,

Corrosion form Uniform - transgranular

Corrosion type ?

MiCorr stratigraphy(ies) – CS

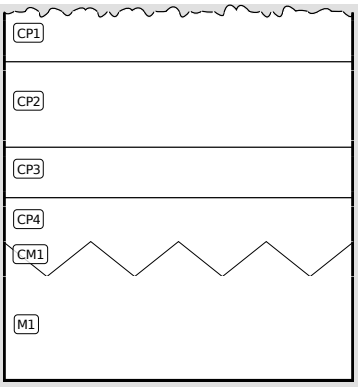

Fig. 4: Stratigraphic representation of the object in cross-section using the MiCorr application. This representation can be compared to Fig. 9.

Synthesis of the binocular / cross-section examination of the corrosion structure

Corrected stratigraphic representation: none

Conclusion

The sword blade is made of a hard, P-rich iron. It displays poor workmanship compared to other Celtic swords. The metal was first hot worked followed by a final cold working. The corrosion layer, typical of terrestrial context, has been partially removed by the conservation treatment. The possible use of air abrasive cleaning with glass beads and aluminium oxide, or the use of abrading tools, could explain the enrichment in Si and Al of the surface.

References

References on object and sample
References object
1. Senn Bischofberger, M. (2005) Das Schmiedehandwerk im nordalpinen Raum von der Eisenzeit bis ins frühe Mittelalter. Internationale Archäologie, Naturwissenschaft und Technologie Bd. 5, (Rahden/Westf.), 30.
References sample
2. Senn Bischofberger, M. (2005) Das Schmiedehandwerk im nordalpinen Raum von der Eisenzeit bis ins frühe Mittelalter. Internationale Archäologie, Naturwissenschaft und Technologie Bd. 5, (Rahden/Westf.), 240-242.
References on analytic methods and interpretation
3. Swiss, A. J. and McDonnell, J.G. (2003) Evidence and interpretation of cold working in ferritic iron. International Conference, Archaeometallurgy in Europe 2003, Proceedings, vol. 1, Milan, 209-217.